AJNR

Size estimation and magnification error in radiographic imaging: implications for classification of arteriovenous malformations.

K Elisevich, I A Cunningham and L Assis

AJNR Am J Neuroradiol 1995, 16 (3) 531-538
http://www.ajnr.org/content/16/3/531

Size Estimation and Magnification Error in Radiographic Imaging: Implications for Classification of Arteriovenous Malformations

Kost Elisevich, Ian A. Cunningham, and Leo Assis

PURPOSE: To assess magnification error in digital subtraction angiography as it pertains to arteriovenous malformation (AVM) size. **METHODS:** A rectangular grid phantom with equally spaced markers mounted in a stereotactic frame was imaged with digital angiographic equipment. The location and orientation of the grid was altered relative to the central plane of the phantom. Both linear and area measurements were made according to the perceived location of phantom markers using a standard catheter calibration technique and compared with stereotactically derived estimates. Finally, a single case example of an angiographically imaged rolandic AVM was used to compare linear dimensions obtained with both described techniques. **RESULTS:** The determination of location and size with standard angiographic imaging is subject to error because of the divergent geometry of the incident x-ray beam. The resulting nonconstant geometric magnification causes errors in linear measurements of 10% to 13% at depths of 7 cm from the calibration plane. Errors in area measurements at the same position increase by 20% to 25%. Measurements of maximum diameter or cross-sectional area may have an additional error when nonspherical objects are inclined to the viewing direction (40% at 45° inclination). These errors are reduced to less than 1 mm using the stereotactic technique. Some commercial angiographic systems have internal software to enable a spatial calibration based on known distances in the image or on the diameter of a catheter. The catheter technique was accurate in the calibration direction (perpendicular to the catheter axis) but had a 12% error in the direction parallel to the catheter because of a nonunity aspect ratio in the video system. Measurement of the dimensions of a rolandic AVM using the catheter calibration technique had an error that ranged from −3% to +26% (standard error, 20%) with respect to the stereotactic technique. **CONCLUSIONS:** Numerous nonstereotactic referential systems for determining linear distances are inherently erroneous by varying degrees compared with the stereotactic technique. Area and volume determinations naturally increase this error further. To the extent that no standardized method for determining linear distances exists, significant variations in estimation of AVM size result. Classification schemes for AVMs have been hampered by this technical error.

Index terms: Arteriovenous malformations; Angiography, technique

AJNR Am J Neuroradiol 16:531–538, March 1995

A standard criterion in the classification of arteriovenous malformations (AVMs) has been some form of size estimation in all reported series. Because of the subjective nature of nidus delineation, it is difficult to draw comparisons among the three standard digital imaging technologies (magnetic resonance [MR] imaging, computed tomography, and cerebral digital subtraction angiography) as to their usefulness in estimating AVM dimension. Computed tomography uses linear (x-ray) projection techniques for image creation, ensuring geometric accuracy between an object and its image. The reliability of MR imaging in location and size estimation, however, is dependent upon the elimination of factors that produce both magnetic field inhomogeneity and signal voids

Received February 16, 1994; accepted after revision September 19.

The financial support of the Sterling-Winthrop Imaging Research Institute is gratefully acknowledged.

From the Department of Neurosurgery, Henry Ford Hospital, Detroit, Mich (K.E.); and the Departments of Clinical Neurological Sciences (Division of Neurosurgery [K.E.]) and Radiology (L.A.) (Imaging Physics [I.A.C.]), Victoria Hospital and the John P. Robarts Research Institute, London, Ontario, Canada.

Address reprint requests to Kost Elisevich, MD, c/o Editorial Office, Department of Neurosurgery, Henry Ford Hospital, 2799 W Grand Blvd, Detroit, MI 48202.

AJNR 16:531–538, Mar 1995 0195-6108/95/1603–0531

Fig 1. Frontal (*A*) and dorsal (*B*) photographic views of a plexiglass phantom grid array housed in an Olivier Bertrand Tipal stereotactic frame. The frontal view displays the y-z plane of the frame, which is orthogonal to the incident x-ray beam in this study. Four fiducial markers on both anterior and posterior surfaces of the frame are used to determine the coordinates of selected grid points in the stereotactic volume. The dorsal view displays the x-z plane of the frame and shows three grid plates at varying x-coordinate values (depths).

caused by complex flow patterns. Various authors have reported coordinate errors of 3 to 5 mm (1–3) using MR imaging. Recently, point-to-point distance variability between computed tomography and MR imaging was reported to be no more than 2 mm in two-dimensional comparison measurements, assuming proper MR machine calibration and correction of nonlinear magnetic field gradients (4). Current volume-rendering algorithms associated with MR imaging and computed tomography are applicable to AVM size estimation; however, an accurate appreciation of arterial feeders, venous drainage vessels, and the often multicompartmental nature of the AVM nidus can be derived only from an angiographic study at present.

This paper addresses error in magnification as it may apply to AVM angiography using standard digital subtraction imaging techniques. There has been considerable variability in reporting of AVM size, with some authors mentioning a magnification factor and others not. Any scheme that reliably measures size must take into consideration the divergent nature of the incident beam, the proximity of the AVM to the image plane, the variability of source-to-image plane distances, and deviation from standard orthogonal projections. Magnification is a function of depth and should, properly, not be expressed as a single value. In addition, commercial angiographic systems may have a nonunity video system aspect ratio, resulting in different pixel sizes in the vertical and horizontal directions. This will also adversely affect size estimations.

All nonstereotactic methods for calibrating the size of intracranial targets have similar shortcomings in that the location of the target is difficult to judge, particularly on initial study. This is in contrast to the commonly used technique of placing a circular or spherical object in the vicinity of the carotid bifurcation for extracranial carotid studies where the anatomic orientation is much clearer. Moreover, the use of a single planar calibration marker as with the latter technique does not address the three-dimensional character of the AVM nidus because it is accurate as a measure of size only in its own calibration plane. Any tilt of the circular marker will render the scaling factor different in the vertical and horizontal directions. In this paper, we report on (*a*) errors in linear dimension measurements, (*b*) errors in area measurements, (*c*) errors in linear measurements based on a commercially available catheter calibration, and (*d*) errors in the measured dimensions of a rolandic AVM.

Methods and Materials

Standard orthogonal projection images of a rectangular grid test phantom housed in a stereotactic frame (Olivier Bertrand Tipal frame, Tipal Instruments, Montreal) containing fiducial markers (Fig 1) were taken using digital imaging equipment commonly used for angiography (Siemens Polytron). The Olivier Bertrand Tipal frame has been described in detail elsewhere (5, 6) and was confirmed to be accurate within 1 mm in our institution. The test phantom construction consisted of plexiglass grid plates with holes in a 2-D matrix of 1-cm spacings. A standard neuroradiographic technique (80 kilovolts [peak], four frames per second) with orthogonal (anteroposterior and lateral) views was used in imaging the phantom with the central ray directed along the x-axis of the frame (Fig 2). The location of a single grid plate was altered along the x-axis by up to 7 cm both anterior and posterior to the central plane. Source-to-frame and source-to-image plane distances were held constant at 68 and 104 cm, respectively, typical of actual usage in a neuroangiographic suite.

Linear Measurements

The apparent distance between each pair of the five grid points (P1 to P5 in Fig 2) decreases as the grid plate is

Fig 2. Schematic diagram illustrating the grid plate in the test phantom. The indicated axes correspond to the frame axes. Measurements were also obtained when the identified five points (*P1* to *P5*) were in a plane at an angle θ with respect to the plane normal to the incident x-ray beam.

moved along the x-axis away from the x-ray source because of decreasing geometric magnification. Measurements taken with respect to perceived (imaged) locations are, therefore, apparent and not necessarily true. The apparent distance relative to that obtained with the grid in the central position, *d,* is given by (see Appendix 1)

$$d = \frac{D}{D + x} \quad (1)$$

where D is the source-to-frame distance and x is the anteroposterior displacement of the grid plate from the central position. Values of d were determined with and without the use of a stereotactic algorithm (7).

Area Measurements

Area measurements were obtained using the outer four grid points to render both real and perceived measures of area at the same grid plate positions. Areas were determined using a vector cross-product technique (see Appendix 2). The area relative to that obtained with the grid plate in the central position, *a,* is given by (see Appendix 1)

$$a = \frac{D^2}{(D + x)^2}. \quad (2)$$

Areas were determined both with and without the stereotactic algorithm (7). In addition, the apparent area $a_t(\theta)$ was determined as the grid plate was tilted by the angle θ (see Fig 2) with respect to the x-ray beam, where

$$a_t(\theta) = a \cos(\theta). \quad (3)$$

Catheter Calibration Measurements

Distances were also determined using commercial software supplied with the angiographic system. With this method, the diameter of a 5.5F catheter placed in the same plane as the grid plates was used as the basis for the spatial calibration. The system software determines the appropriate calibration factor by making a least-squares fit of the theoretical catheter profile to the actual profile in the image. Using a vertical catheter in an angiographic image of the test phantom, distances were determined in both parallel and perpendicular directions.

Fig 3. Dimensions determined directly from an image are dependent on the depth of the target in the field. This graph shows the measured distance between two grid points in the same plate, normalized to unity at the phantom center (plate position, 0 cm) for a range of grid plate depths. The ordinate represents the relative error in the perceived distances. Units along the abscissa represent plate positions posterior to (negative) and anterior to (positive) the phantom center. The theoretical *solid line* is given by equation 1.

Rolandic AVM Measurements

A digital subtraction angiogram of a patient harboring a left rolandic AVM was obtained in preparation for stereotactic radiosurgery. Linear dimensions of the lesion were determined with software on the angiographic system using a catheter in the left internal carotid artery as the basis for the spatial calibration. These results were compared with the same dimensions in the same images obtained using a stereotactic algorithm as a typical case example of the error inherent in size estimation by nonstereotactic means.

Results

Linear Measurements

Dimensions within the y-z plane of the stereotactic frame determined from image data varied according to location (depth) of the rectangular plate within the frame. The measured distance between two grid points within the plane of a single grid plate, normalized to unity at the phantom center, is shown in Figure 3 for a range of plate depths (x). The results were consistent with theoretical expectations given by equation 1, as indicated by the *solid line*.

The error relative to the known physical dimensions of the plexiglass test phantom was

Fig 4. Errors in area determination are more severe. This graph shows the area of a region defined by four selected grid points in the same plate situated orthogonally with respect to the incident x-ray normalized to unity at the phantom center (plate position, 0 cm). The ordinate represents the relative error in perceived distances between grid points. Units along the abscissa represent plate positions posterior to (negative) and anterior to (positive) the phantom center. The theoretical *solid line* is given by equation 2.

determined to be 10% to 13% at a depth of 7 cm from the frame (and phantom) center, consistent with equation 1. This error was reduced to less than 1 mm using the stereotactic algorithm.

Area Measurements

Figure 4 shows the relative size of the same region (normalized to unity at the phantom center) as a function of grid position (x) within the frame. The *solid line* indicates the theoretical relationship given by equation 2. The area error was 20% to 25% at a depth of 7 cm from the phantom center. Using the stereotactic technique, these errors were reduced to less than 1 mm^2.

Further area determinations were rendered in planes at an angle θ to the plane perpendicular to the incident x-ray beam by tilting the grid plate (Fig 2). Figure 5 shows area determinations in a plane centered at phantom center for a range of inclinations. The results are consistent with equation 3 (*solid line*). Inclined plane area determinations increased the error further when compared to a central plane orthogonal to the incident x-ray beam. For example, a 40% error in area determination was evident at a 45° inclination.

Catheter Calibration Measurements

The aspect ratio of the digital subtraction angiography system (ie, ratio of pixel physical width to pixel physical height) was measured to

Fig 5. The error in measurement of area is worsened when the target is in a plane inclined at an angle θ to the direction of the central ray. This graph shows the area of a region defined by four selected grid points in the same plate situated at phantom center and rotated along an axis orthogonal to the central ray, normalized to unity at $\theta = 0°$. The theoretical *solid line* is given by equation 3.

be 1.14. The resultant error is attributable to different relative horizontal-scan and vertical-sweep rates in the video camera and digitizer circuitry, which are normally adjusted by the service representative during system installation or calibration. As a result, measurements made in the direction parallel to the catheter direction will be in error by 14% with respect to measurements made in the perpendicular direction. This error was observed experimentally and is shown in Table 1.

Rolandic AVM Measurements

The difficulties encountered in size estimation during angiography are illustrated in a single case example of a cerebral AVM studied by digital angiography preparatory to stereotactic radiosurgery. The linear dimensions of a left dorsomedial rolandic AVM determined by a neuroradiologist using software on a Siemens Polytron angiographic system and a catheter calibration technique (Fig 6) are summarized in Table 2. Maximal linear dimensions in the lat-

TABLE 1: Accuracy of the catheter technique perpendicular and parallel to the catheter direction

Direction	Actual, mm	Catheter Method, mm	Error, %
Perpendicular	80.0	79.5	−1
Parallel	80.0	69.8	−13

Fig 6. Lateral digital subtraction angiographic projections of a dorsomedial rolandic AVM following left carotid injection of contrast. Linear dimensions marked on this image were determined using software on a Siemens Polytron angiographic system in the calibration plane determined by the neuroradiologist. A stereotactic algorithm was used subsequently to calculate the same AVM dimensions.

eral view exceeded 44 mm. When the same AVM was analyzed with the stereotactic algorithm using the same digital subtraction angiographic images, maximal dimensions did not exceed 37 mm. The discrepancy between the catheter and stereotactic techniques in both lateral and posteroanterior views using the same landmarks (Fig 6) ranged from −3% to +26%, with a standard error of 20%.

TABLE 2: Rolandic AVM dimensions determined with the catheter and stereotactic techniques

Line*	Catheter Method, mm	Stereotactic Method, mm	Error, %
Lateral			
a	44.4	36.5	+22
b	32.1	29.2	+10
c	36.8	28.0	+31
d	41.3	32.8	+26
Posteroranterior			
e	37.1	38.1	−3
f	36.2	41.8	−13

* The identification letters correspond to dimensions indicated in Figure 7.

Discussion

Variability in magnification from one angiographic study to the next and from one projection to the next is influenced by source-to-patient distances and lesion position within the brain. Such variability, when coupled with the error in assessing the degree of magnification in a given projection, hampers any attempt at standardizing size estimation of AVMs. The proximity of a vascular lesion to the image plane will naturally alter the size of its image. Thus, the size of a lesion situated in the convexity of the right cerebral hemisphere should have a much different mean correction factor than the same lesion situated in the convexity of the left hemisphere when imaged in the lateral projection. Attempts at standardizing size in angiographic studies by introducing a calibration mark of known dimension into the imaged field external to the cranium suffer the same flaw. Parallax error will further influence the estimation in this circumstance, as the calibration mark is commonly far removed from the central ray. The diverging geometry of the incident x-ray beam also dictates that magnification is a function of depth and therefore is not a constant value. The stereotactic method was originally designed to overcome the inherent problems of 3-D point determination in projectional neuroradiography and is based upon sound physical design and mathematical principles (8).

Although other factors exclusive of nonconstant geometric magnification such as parallax, pincushion distortion in the image intensifier and video system, nidus definition, surface irregularity, and nonuniform contrast transit times and clearance will hinder proper size estimation, we have chosen to study only the magnification factor as it is the most commonly expressed corrective parameter in angiographic studies of vascular malformations. Many groups have categorized AVMs by size (9–19). Most have referred to the maximum linear dimension from angiographic study in size estimation. Such determinations are suitable for spherical AVMs, in which case our estimate of a 10% to 13% maximal linear error would render only a 5- to 7-mm overestimate of size for a 5.0-cm nidus. AVMs, however, are not of uniform shape, and therefore cannot be readily compared by linear dimension. The orientation of the long axis of the AVM nidus may introduce a further limitation of nonstereotactic angiography. This

is exemplified in the case in which the long axis is oriented at 45° to both orthogonal views and a 41% error results in estimating its length (20). Yet, to proceed to higher dimensional categorizations of size necessarily introduces further error in magnitude as seen in this study. Error in estimating the cross-sectional area in a plane orthogonal to the incident x-ray beam could increase by 20% to 25%. Such estimates worsen considerably when the cross-sectional area is inclined relative to the incident x-ray beam.

Volume estimation has been suggested as the preferred method for AVM size categorization (11, 21). This clearly allows greater universality in comparing AVM size, as two geometrically different AVMs with identical maximal linear dimensions are likely to have substantially different volumes. The majority of publications related to clinical outcome with regard to cerebral AVMs have addressed size by maximal linear dimension rather than cross-sectional area or volume. The incidence of postoperative breakthrough hemorrhage has been found to be significantly higher following resections of AVMs larger than 4 to 5 cm (14, 16, 17, 22). Overall postoperative outcome has been shown to be significantly better for AVMs smaller than 4 cm (17). The size of cerebral AVMs has also been correlated with surrounding (penumbral) cerebral blood flow and severity of dysautoregulation (13, 23, 24).

Aside from factors predicting postoperative morbidity, the efficacy of stereotactic radiosurgery in eliminating AVMs has also been related to the size of the AVM nidus, using maximal linear dimensions determined from conventional angiography. Those malformations measuring less than 3 cm have been found to respond favorably to radiosurgery, with complete obliteration noted in 80% to 90% of cases after a 2-year latency (25, 26).

The resolution of MR imaging afforded by nonreformatted data acquisition and the appreciation of anatomical detail of central nervous system tissue in the immediate vicinity of an AVM gives this imaging modality some advantage in treatment planning. The definition of an AVM nidus on projectional images is subject to individual bias to some degree, giving rise to interobserver variability in interpretation. The greater the penumbra of arterioarterial connections and the greater the nidus irregularity, the more such variability will occur. Although it was not our intent to examine such factors in this work, this important aspect of AVM size estimation will require standardization, by consensus, of its own. Noorbehesht et al (27) have suggested that MR imaging is superior to angiography in delineating the AVM nidus for size determination, citing the fact that its cross-sectional nature allowed one to distinguish between nidus and overlapping veins. The latter were believed to add erroneously to nidus size on projectional imaging. Although rapidly sequenced static angiographic images may not always isolate the nidus exclusively in fast-flow AVMs, it is unlikely the nidus would not be properly appreciated with computer-assisted dynamic imaging (28). This allows one to interpolate and replay a sequence of images with an effective frame rate of 30 frames per second to provide the purest view of the nidus. Moreover, the compartmental nature of some AVMs can be appreciated only with angiography through sequential imaging or selective injections of unilateral or bilateral carotid and/or vertebral arteries. It also remains difficult to distinguish vessels unique to the nidus from those that are "en passage," whether MR imaging or angiography is used. Hence the two imaging modalities are likely to remain married in the investigation of AVMs and in their treatment planning.

Because size has factored significantly in AVM classification, prognostication, and therapeutic decision making, it is appropriate that a universally and reasonably accurate standard approach be taken when measurements are obtained from angiograms. Because it appears that volume determination is the best such standard for size, it is important to draw attention to the magnitude of error inherent in volume estimation given the error observed in cross-sectional area determination in the absence of stereotactic technology. Conservative estimates of such error would approach 40%, making it virtually impossible to allocate AVMs into distinctive size categories. Deviation of the major axis of a nonspherical nidus from the view (central ray) axis at an acute angle, coupled with the displacement of the nidus center from the central ray, may at times impose considerable limitations on our ability to estimate nidus size. A means of overcoming this is provided by stereotactic angiographic imaging, in which nidus size may be determined with a measuring algorithm negating the influence of magnification

Fig 7. The perceived distance between two points $l1$ is related to the actual distance c, source-frame distance D, and plate position x as shown.

entirely. Limitations remain in estimating AVM size with two orthogonal views. Departure from spherical geometry also introduces difficulties in conceptualizing overall shape (20). In fact, significant irregularity and multicompartmentalization present the most important sources of error in precision volume rendering. Interobserver variability adds further to the difficulties encountered in size estimation and emphasizes the need for careful review of fast-sequenced images to reduce the overestimation of size attributable to the penumbra of arterioarterial connections. Such problems may be overcome eventually by stereotactic digitized dynamic angiographic imaging and an interactive volume-rendering algorithm.

Acknowledgments

We thank S. Thielen for assistance in the experimental work and W. Ryan and H. Lai for manuscript preparation.

Appendix 1

As points *P1* and *P2* in the test phantom are moved a distance x away from the x-ray source, the resulting perceived distance between them in the image plane increases from $l1$ to $l2$ (see Fig 7). The relative increase, normalized to unity at $x = 0$, is determined using similar triangles shown in Figure 7 and is given by

$$\text{A1-1)} \qquad d = \frac{l1}{l2} = \frac{c/(D+x)}{c/D} = \frac{D}{D+x}.$$

Appendix 2

The area a encompassed by four points in three dimensions can be expressed as the vector cross-product (29)

$$\text{A2-1)} \qquad a = \frac{1}{2}[|V_{1,2} \times V_{1,4}| + |V_{3,4} \times V_{3,2}|],$$

where

$$\text{A2-2)} \qquad V_{1,2} \times V_{1,4} = [(x_2 - x_1)^2 + (y_2 - y_1)^2 + (z_2 - z_1)^2][(x_4 - x_1)^2 + (y_4 - y_1)^2 + (z_4 - z_1)^2] - [(x_2 - x_1)(x_4 - x_1) + (y_2 - y_1)(y_4 - y_1) + (z_2 - z_1)(z_4 - z_1)]^2$$

and

$$\text{A2-3)} \qquad V_{3,4} \times V_{3,2} = [(x_4 - x_3)^2 + (y_4 - y_3)^2 + (z_4 - z_3)^2][(x_2 - x_3)^2 + (y_2 - y_3)^2 + (z_2 - z_3)^2] - [(z_4 - x_3)(x_2 - x_3) + (y_4 - y_3)(y_2 - y_3) + (z_4 - z_3)(z_2 - z_3)]^2.$$

The coordinates (x_i, y_i, z_i) correspond to those of the ith point in Figure 2. Real areas (mm^2) are determined with the stereotactic coordinates. Perceived areas ($pixels^2$) are determined with pixel coordinates by setting all x coordinates to a constant.

References

1. Bradford R, Thomas DGT, Bydder GM. MR imaging-directed stereotactic biopsy of cerebral lesions. *Acta Neurochir Suppl (Wien)* 1987;39:25–27
2. Heilbrun MP, Sunderland PM, McDonald PR, Wells TH Jr, Cosman E, Ganz E. Brown-Roberts-Wells stereotactic frame modifications to accomplish magnetic resonance imaging guidance in three planes. *Appl Neurophysiol* 1987;50:143–152
3. Villemure JG, Marchand E, Peters TM, Leroux G, Olivier A. Magnetic resonance imaging stereotaxy: recognition and utilization of the commissures. *Appl Neurophysiol* 1987;50:57–62
4. Kondziolka D, Dempsey PK, Lunsford LD, et al. A comparison between magnetic resonance imaging and computed tomography for stereotactic coordinate determination. *Neurosurgery* 1992;30: 402–407
5. Olivier A, Bertrand G. Stereotaxic device for percutaneous twist-drill insertion of depth electrodes and for brain biopsy (technical note). *J Neurosurg* 1982;56:307–308
6. Olivier A, Bertrand G, Peters T. Stereotactic systems and procedures for depth electrode placement: technical aspects. *Appl Neurophysiol* 1983;46:37–40
7. Peters TM, Clark JA, Olivier A, et al. Integrated stereotaxic imaging with CT, MR imaging and digital subtraction angiography. *Radiology* 1986;161:821–826
8. Bergstrom M, Greitz T, Steiner L. An approach to stereotaxic radiography. *Acta Neurochir (Wien)* 1980;54:157–165
9. Drake CG. Cerebral arteriovenous malformations: considerations for and experience with surgical treatment in 166 cases. *Clin Neurosurg* 1979;26:145–208

10. Guidetti B, Delitala A. Intracranial arteriovenous malformations: conservative and surgical treatment. *J Neurosurg* 1980;53:149–152
11. Luessenhop AJ, Gennarelli TA. Anatomical grading of supratentorial arteriovenous malformations for determining operability. *Neurosurgery* 1977;1:30–35
12. Luessenhop AJ, Rosa L. Cerebral arteriovenous malformations: indications for and results of surgery and the role of intravascular techniques. *J Neurosurg* 1984;60:14–22
13. Marks MP, O'Donahue J, Fabrikant JI, et al. Cerebral blood flow evaluation of arteriovenous malformations with stable xenon CT. *AJNR Am J Neuroradiol* 1988;9:1169–1175
14. Shi Y, Chen XC. A proposed scheme for grading intracranial arteriovenous malformations. *J Neurosurg* 1986;65:484–489
15. Spetzler RF, Martin NA. A proposed grading system for arteriovenous malformations. *J Neurosurg* 1986;65:476–483
16. Sugita K, Takemae N. Surgery of large arteriovenous malformations. *Neurosurgery* 1988;7:35–41
17. Tamaki N, Ehara K, Lin T, et al. Cerebral arteriovenous malformations: factors influencing the surgical difficulty and outcome. *Neurosurgery* 1991;29:856–861
18. Waltimo O. The relationship of size, density and localization of intracranial arteriovenous malformations to the type of initial symptom. *J Neurol Sci* 1973;19:13–19
19. Wilson CB, U HS, Domingue J. Microsurgical treatment of intracranial vascular malformations. *J Neurosurg* 1979;51:446–454
20. Bova FJ, Friedman WA. Stereotactic angiography: an inadequate database for radiosurgery? *Int J Radiat Oncol Biol Phys* 1991;20:891–895
21. Pasqualin A, Barone G, Cioffi F, Rosta L, Scienza R, Da Pian R. The relevance of anatomic and hemodynamic factors to a classification of cerebral arteriovenous malformations. *Neurosurgery* 1991;28:370–379
22. Tamaki N, Lin T, Asada M, et al. Modulation of the blood flow following excision of a high flow cerebral arteriovenous malformation. *J Neurosurg* 1990;72:509–512
23. Barnett GH, Little JR, Ebrahim ZY, Jones SC, Friel HT. Cerebral circulation during arteriovenous malformation operation. *Neurosurgery* 1987;20:836–842
24. Pertuiset B, Ancri D, Arthuis F, Basset JY, Fusciardi J, Nakano H. Shunt-induced haemodynamic disturbances in supratentorial arteriovenous malformations. *J Neuroradiol* 1985;12:165–178
25. Betti O, Munari C, Rosler R. Stereotactic radiosurgery with the linear accelerator: treatment of arteriovenous malformations. *Neurosurgery* 1989;24:11–321
26. Steiner L. Radiosurgery in cerebral arteriovenous malformations. In: Fine JM, Flamm ES, eds. *Cerebrovascular Surgery*. Vol 4. New York: Springer-Verlag, 1985:1161–1215
27. Noorbehesht B, Fabrikant JI, Enzmann DR. Size determination of supratentorial arteriovenous malformations by MR, CT and angio. *Neuroradiology* 1987;29:512–518
28. Cunningham IA, Elisevich K, Assis L, Thielen S. Dynamic angiographic imaging of arteriovenous malformations. *Radiology* 1992;185 (Suppl):160
29. Davis HF, Snider AD (eds). *Introduction to Vector Analysis*. 3rd ed. Boston: Allyn and Bacon Inc, 1975

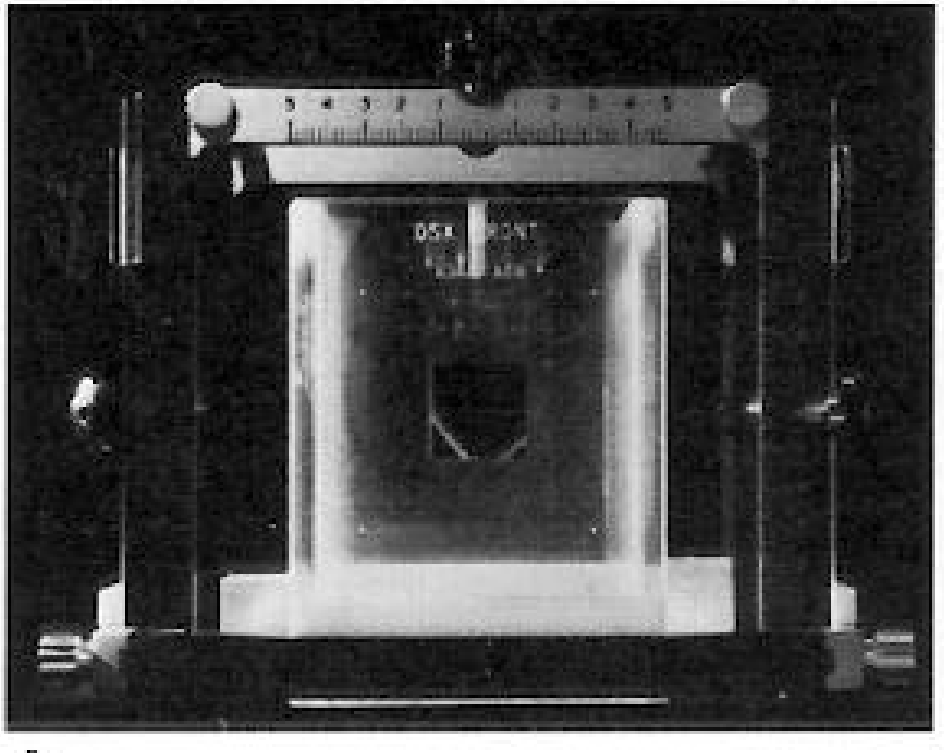

A

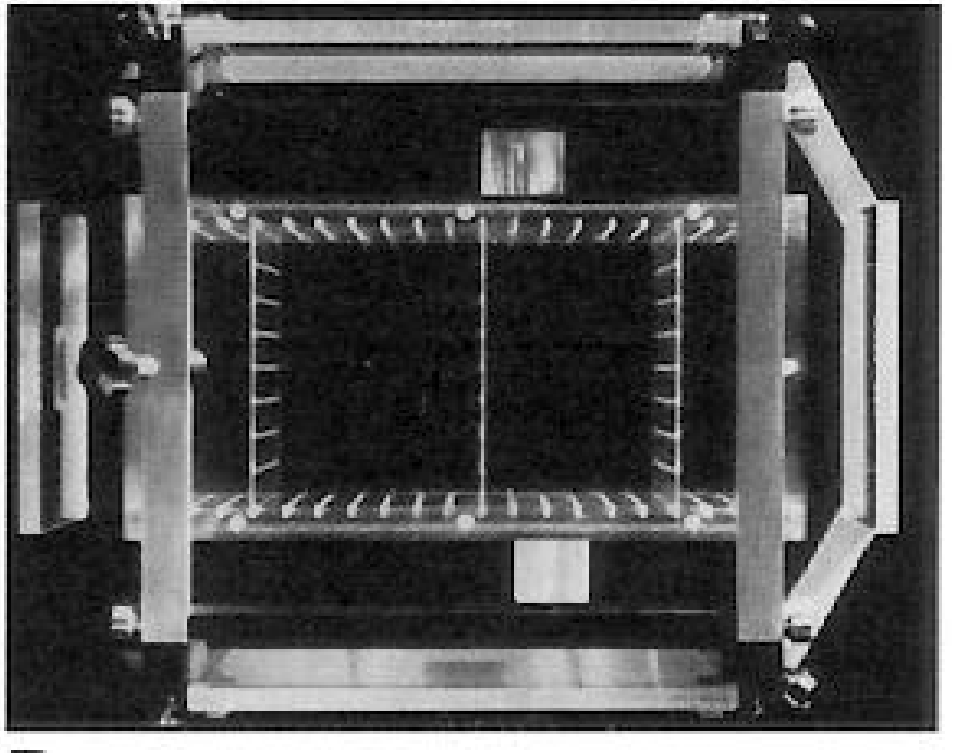

B

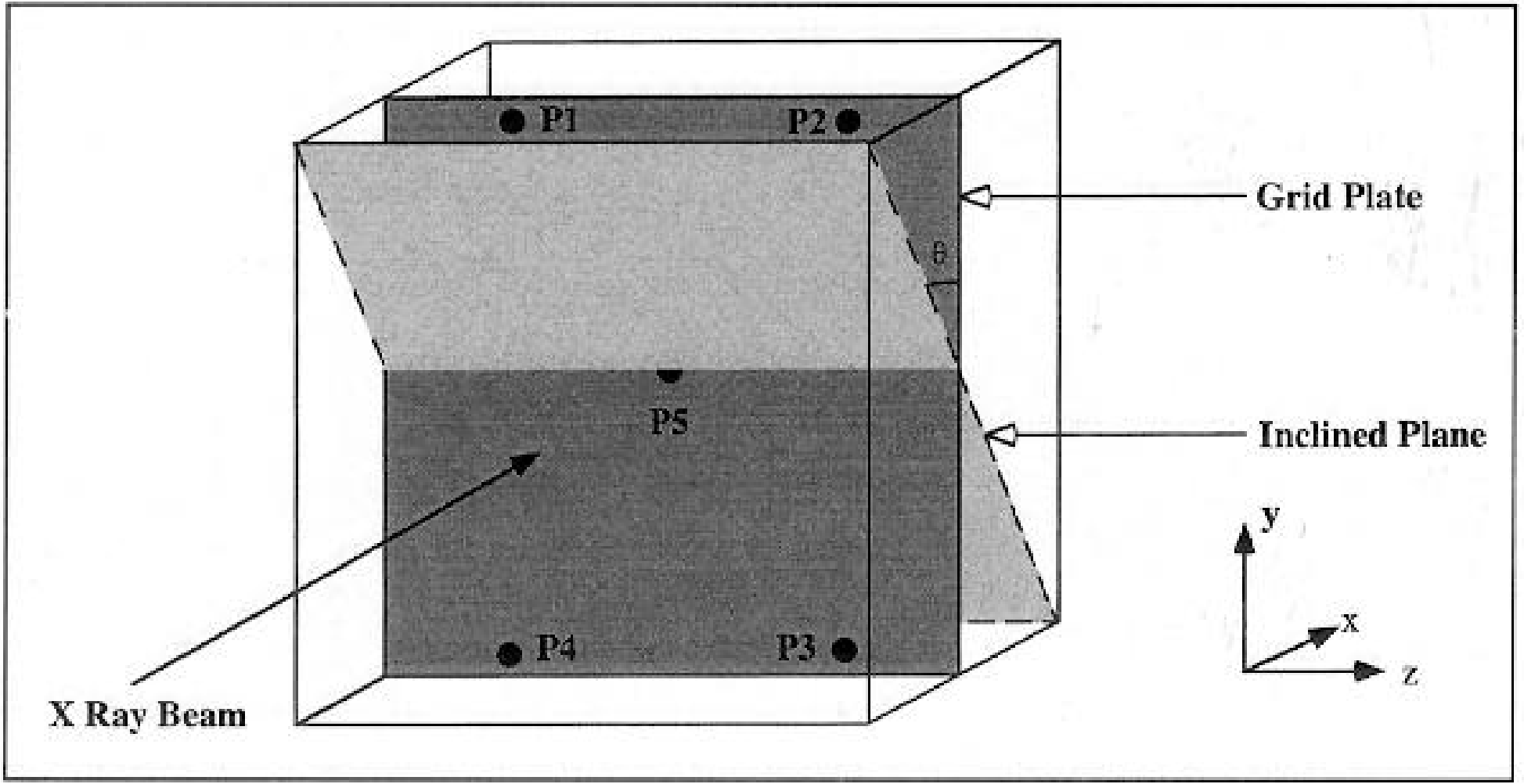
P1
P2
Grid Plate
θ
P5
Inclined Plane
y
x
z
P4
P3
X Ray Beam

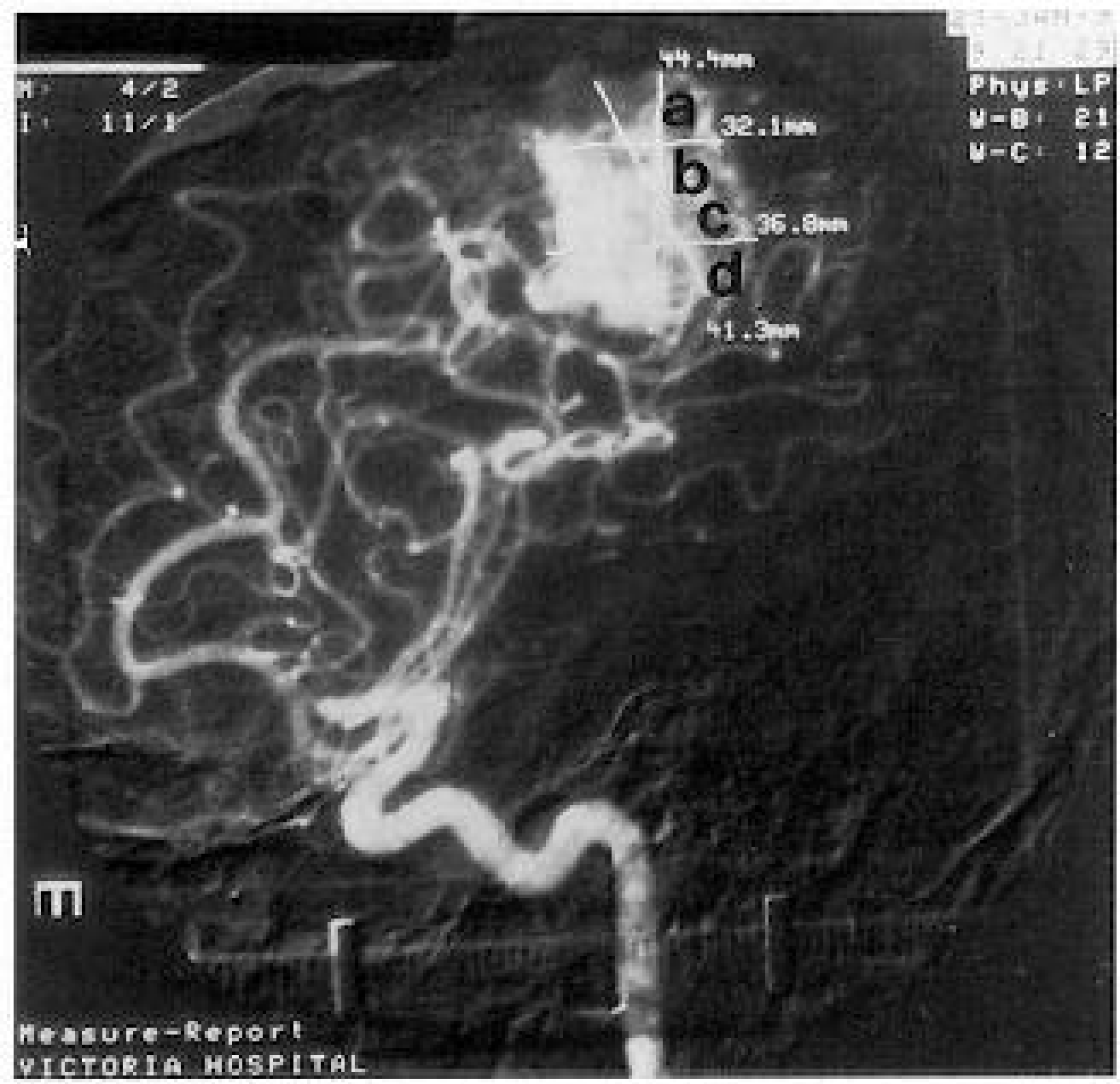
H: 4/2
I: 11/1
44.4mm
a
32.1mm
b
c
35.8mm
d
41.3mm
Phys·LP
U-B: 21
U-C: 12
Measure-Report
VICTORIA HOSPITAL

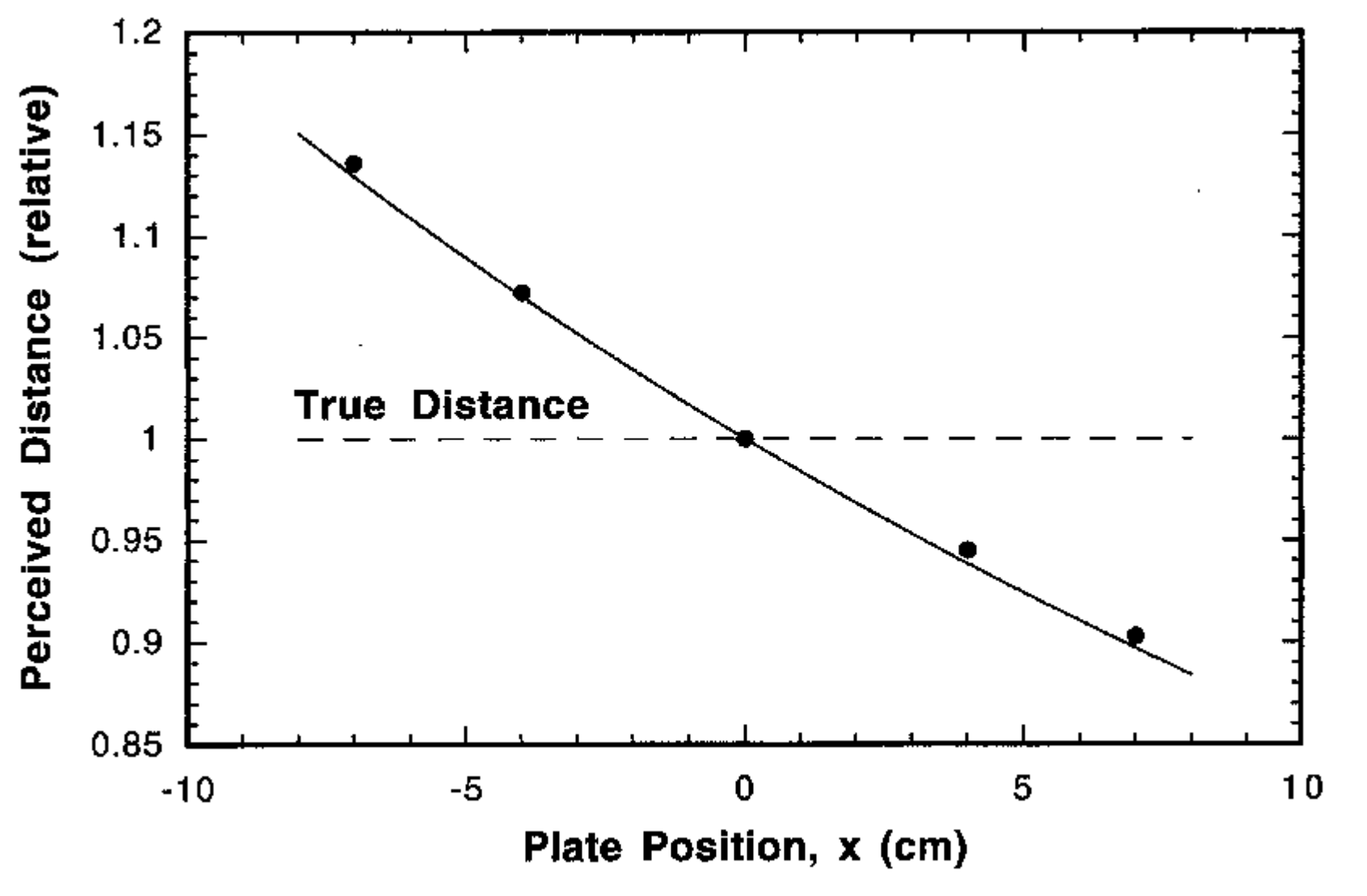
1.2
1.15
1.1
1.05
1
0.95
0.9
0.85
Perceived Distance (relative)
True Distance
-10
-5
0
5
10
Plate Position, x (cm)

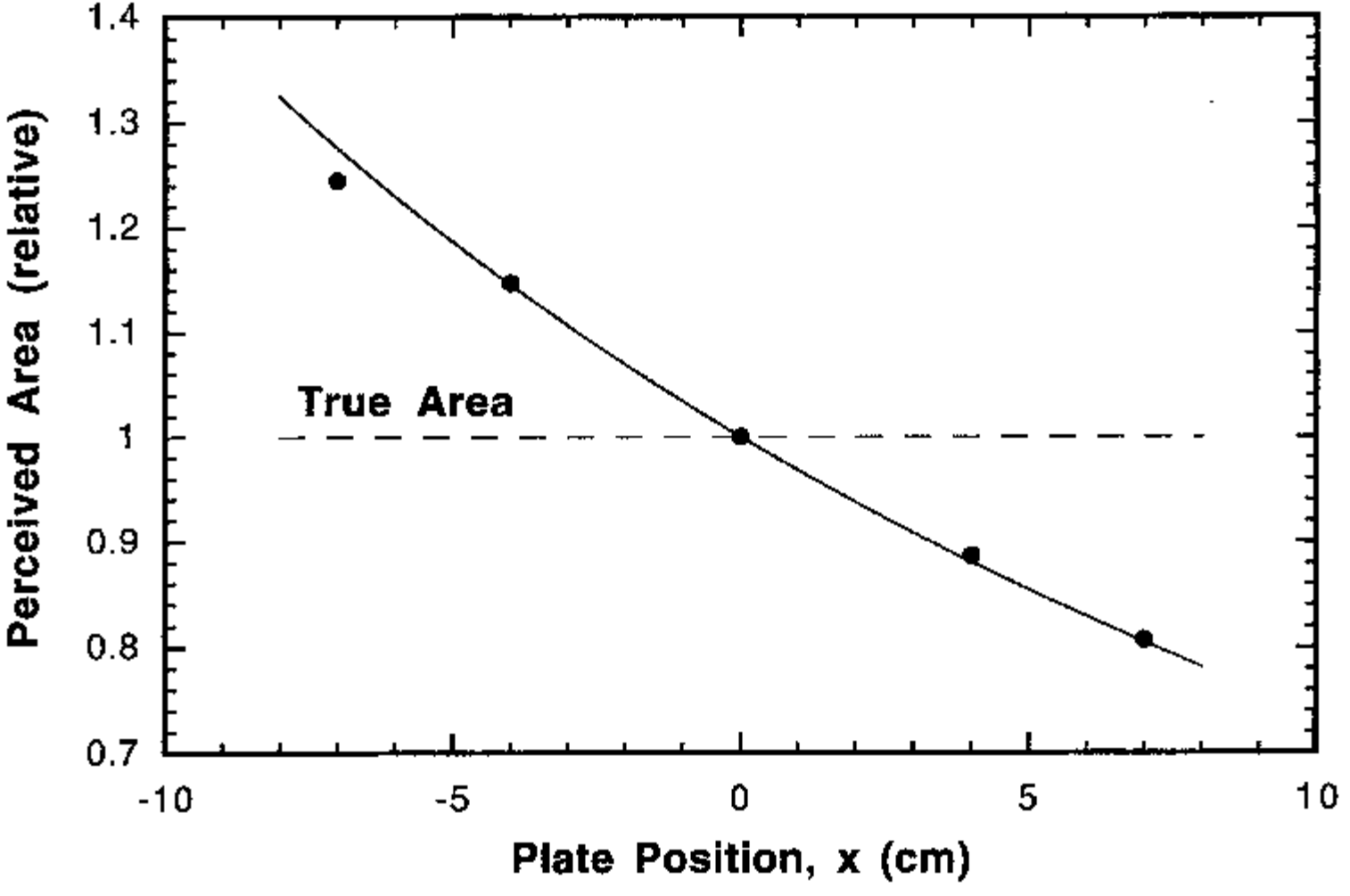
Perceived Area (relative)
1.4
1.3
1.2
1.1
1
0.9
0.8
0.7
True Area
-10
-5
0
5
10
Plate Position, x (cm)

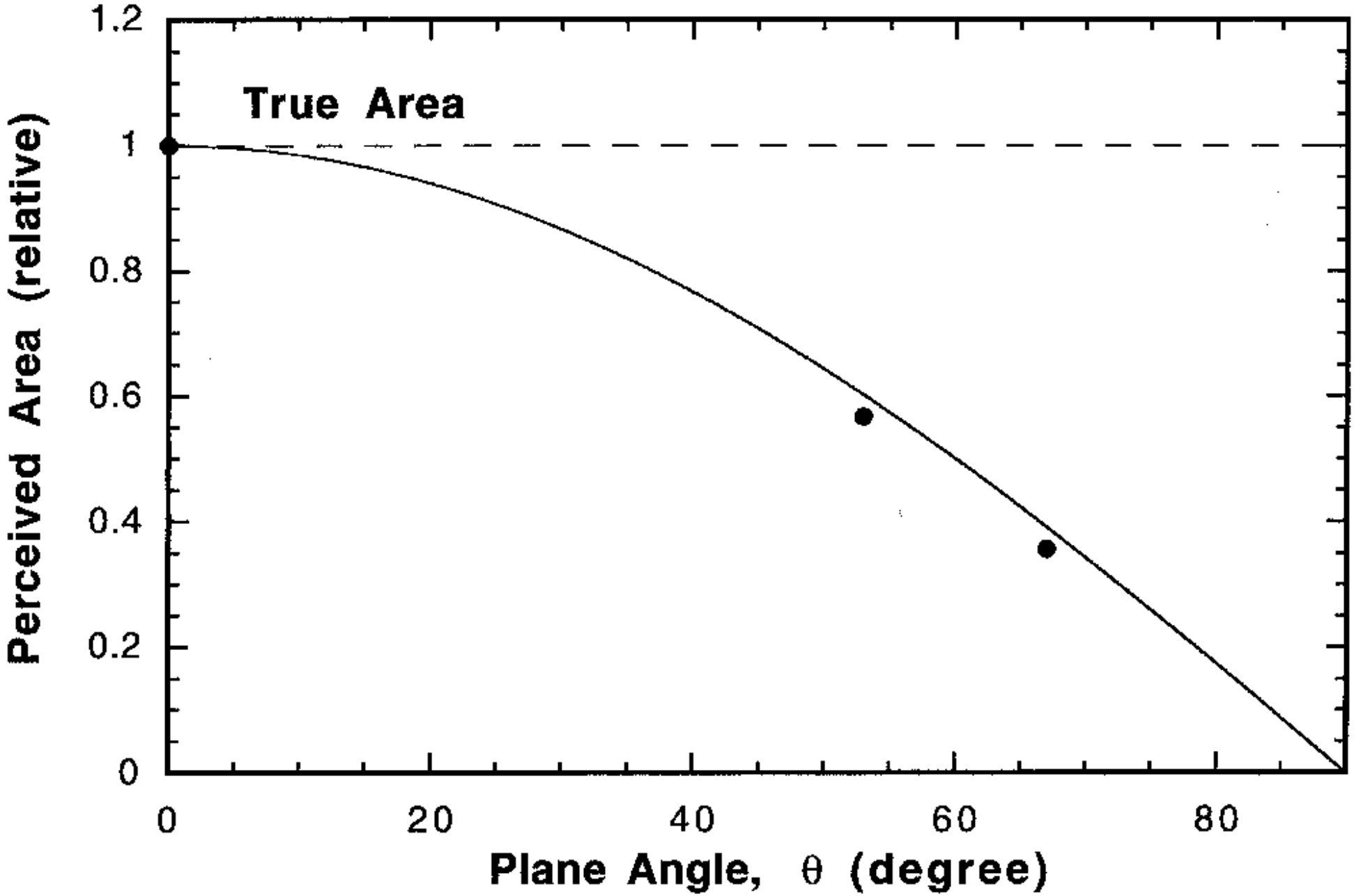
True Area
Perceived Area (relative)
1.2
1
0.8
0.6
0.4
0.2
0
0
20
40
60
80
Plane Angle, θ (degree)

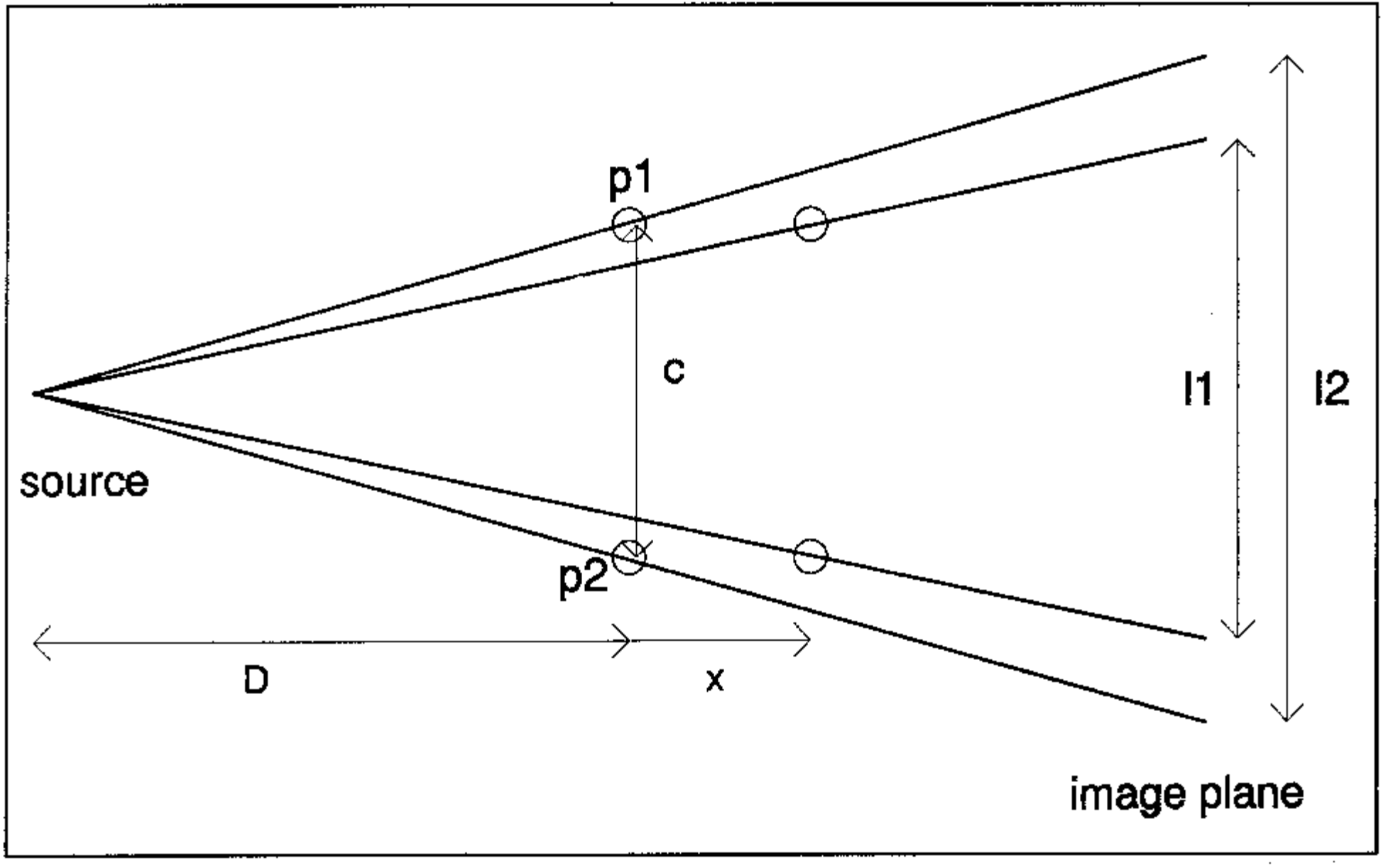
p1
c
l1
l2
source
p2
D
x
image plane